0

Multifractal Turbulence in the Heliosphere

Wiesław M. Macek
Faculty of Mathematics and Natural Sciences, Cardinal Stefan Wyszyński University and Space Research Centre, Polish Academy of Sciences Poland

1. Introduction

The aim of the chapter is to give an introduction to the new developments in turbulence using nonlinear dynamics and multifractals. To quantify scaling of turbulence we use a generalized two-scale weighted Cantor set (Macek & Szczepaniak, 2008). We apply this model to intermittent turbulence in the solar wind plasma in the inner and the outer heliosphere at the ecliptic and at high heliospheric latitudes and even in the healiosheath, beyond the termination shock. We hope that the generalized multifractal model will be a useful tool for analysis of intermittent turbulence in the heliospheric plasma. We thus believe that multifractal analysis of various complex environments can shed light on the nature of turbulence.

1.1 Chaos and Fractals Basics

Nonlinear dynamical systems are often highly sensitive to initial conditions resulting in chaotic motion. In practice, therefore, the behavior of such systems cannot be predicted in the long term, even though the laws of dynamics unambiguously determine its evolution. Chaos is thus a non-periodic long-term behavior in a deterministic system that exhibits sensitivity to initial conditions. Yet we are not entirely without hope here in terms of predictability, because in a dissipative system (with friction) the trajectories describing its evolution in the space of system states asymptotically converge towards a certain invariant set, which is called an attractor; strange attractors are fractal sets (generally with a fractal dimension) which exhibit a hidden order within the chaos (Macek, 2006b).
We remind that a fractal is a rough or fragmented geometrical object that can be subdivided in parts, each of which is (at least approximately) a reduced-size copy of the whole. Strange attractors are often fractal sets, which exhibits a hidden order within chaos. Fractals are generally *self-similar* and independent of scale (generally with a particular fractal dimension). A multifractal is an object that demonstrate various self-similarities, described by a multifractal spectrum of dimensions and a singularity spectrum. One can say that self-similarity of multifractals is point dependent resulting in the singularity spectrum. A multifractal is therefore in a certain sens like a set of intertwined fractals (Macek & Wawrzaszek, 2009).

1.2 Importance of Multifractality

Starting from seminal works of Kolmogorov (1941) and Kraichnan (1965) many authors have attempted to recover the observed scaling laws, by using multifractal phenomenological models of turbulence describing distribution of the energy flux between cascading eddies at various scales (Carbone, 1993; Frisch, 1995; Meneveau & Sreenivasan, 1987). In particular, mul-

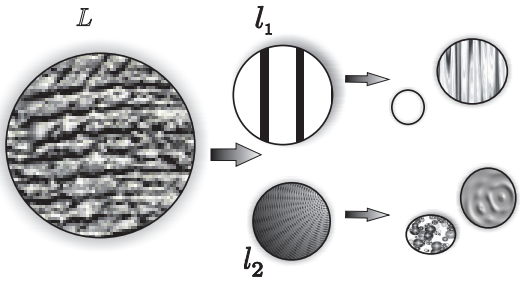

Fig. 1. Schematics of binomial multiplicative processes of cascading eddies.

tifractal scaling of this flux in solar wind turbulence using Helios (plasma) data in the inner heliosphere has been analyzed by Marsch et al. (1996). It is known that fluctuations of the solar magnetic fields may also exhibit multifractal scaling laws. The multifractal spectrum has been investigated using magnetic field data measured *in situ* by Advanced Composition Explorer (ACE) in the inner heliosphere (Macek & Wawrzaszek, 2011a) by Voyager in the outer heliosphere up to large distances from the Sun (Burlaga, 1991; 1995; 2001; 2004; Macek & Wawrzaszek, 2009) and even in the heliosheath (Burlaga & Ness, 2010; Burlaga et al., 2006; 2005; Macek et al., 2011).

To quantify scaling of solar wind turbulence we have developed a generalized two-scale weighted Cantor set model using the partition technique (Macek, 2007; Macek & Szczepaniak, 2008), which leads to complementary information about the multifractal nature of the fluctuations as the rank-ordered multifractal analysis (cf. Lamy et al., 2010). We have investigated the spectrum of generalized dimensions and the corresponding multifractal singularity spectrum depending on one probability measure parameter and two rescaling parameters. In this way we have looked at the inhomogeneous rate of the transfer of the energy flux indicating multifractal and intermittent behavior of solar wind turbulence. In particular, we have studied in detail fluctuations of the velocity of the flow of the solar wind, as measured in the inner heliosphere by Helios (Macek & Szczepaniak, 2008), and ACE (Szczepaniak & Macek, 2008), and Voyager in the outer heliosphere (Macek & Wawrzaszek, 2009; Macek & Wawrzaszek, 2011b), including Ulysses observations at high heliospheric latitudes (Wawrzaszek & Macek, 2010).

2. Methods for Phenomenological Turbulence Model

2.1 Turbulence Cascade Scenario

In this chapter we consider a standard scenario of cascading eddies, as schematically shown in Figure 1 (cf. Meneveau & Sreenivasan, 1991). We see that a large eddy of size L is divided into two smaller *not necessarily equal* pieces of size l_1 and l_2. Both pieces may have different probability measures, p_1 and p_2 as indicated by the different shading. At the n-th stage we have 2^n various eddies. The processes continue until the Kolmogorov scale is reached (cf. Macek, 2007; Macek et al., 2009; Meneveau & Sreenivasan, 1991). In particular, space filling turbulence could be recovered for $l_1 + l_2 = 1$ (Burlaga et al., 1993). Ideally, in the inertial region of the system of size L, $\eta \ll l \ll L = 1$ (normalized), the energy is not allowed to be dissipated directly, assuming $p_1 + p_2 = 1$, until the Kolmogorov scale η is reached. However, in this range at each n-th step of the binomial multiplicative process, the flux of kinetic energy

density ε transferred to smaller eddies (energy transfer rate) could be divided into nonequal fractions p and $1-p$.

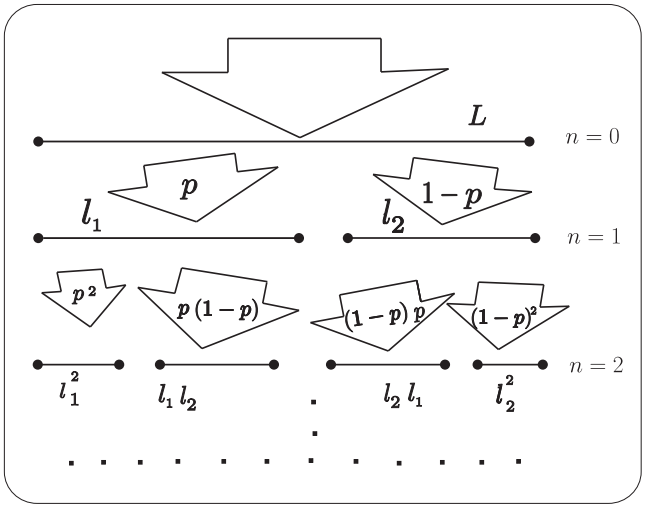

Fig. 2. Two-scale weighted Cantor set model for asymmetric solar wind turbulence.

Naturally, this process can be described by the generalized weighted Cantor set as illustrated in Figure 2, taken from (Macek, 2007). In the first step of the two-scale model construction we have two eddies of sizes $l_1 = 1/r$ and $l_2 = 1/s$, satisfying $p/l_1 + (1-p)/l_2 = 1$, or equivalently $rp + s(1-p) = 1$. Therefore, the initial energy flux ε_0 is transferred to these eddies with the different proportions: $rp\varepsilon_0$ and $s(1-p)\varepsilon_0$. In the next step the energy is divided between four eddies as follows: $(rp)^2\varepsilon_0$, $rsp(1-p)\varepsilon_0$, $sr(1-p)p\varepsilon_0$, and $s^2(1-p)^2\varepsilon_0$. At nth step we have $N = 2^n$ eddies and partition of energy ε can be described by the relation (Burlaga et al., 1993):

$$\varepsilon = \sum_{i=1}^{N} \varepsilon_i = \varepsilon_0 (rp + s(1-p))^n = \varepsilon_0 \sum_{k=0}^{n} \binom{n}{k} (rp)^{(n-k)} (s(1-p))^k. \tag{1}$$

2.2 Comparison With the P-Model

The multifractal measure (Mandelbrot, 1989) $\mu = \varepsilon / \langle \varepsilon_L \rangle$ (normalized) on the unit interval for (a) the usual one-scale p-model (Meneveau & Sreenivasan, 1987) and (b) the generalized two-scale cascade model is shown in Figure 3 ($n = 7$) taken from (Macek & Szczepaniak, 2008). It is worth noting that intermittent pulses are much stronger for the model with two different scaling parameters. In particular, for non space-filling turbulence, $l_1 + l_2 < 1$ one still could have a multifractal cascade, even for unweighted (equal) energy transfer, $p = 0.5$. Only for $l_1 = l_2 = 0.5$ and $p = 0.5$ there is no multifractality.

2.3 Energy Transfer Rate and Probability Measure

In the first step of our analysis we construct multifractal measure (Mandelbrot, 1989) defining by using some approximation the transfer rate of the energy flux ε in energy cascade (Macek & Wawrzaszek, 2009; Wawrzaszek & Macek, 2010). Namely, given a turbulent eddy of size l

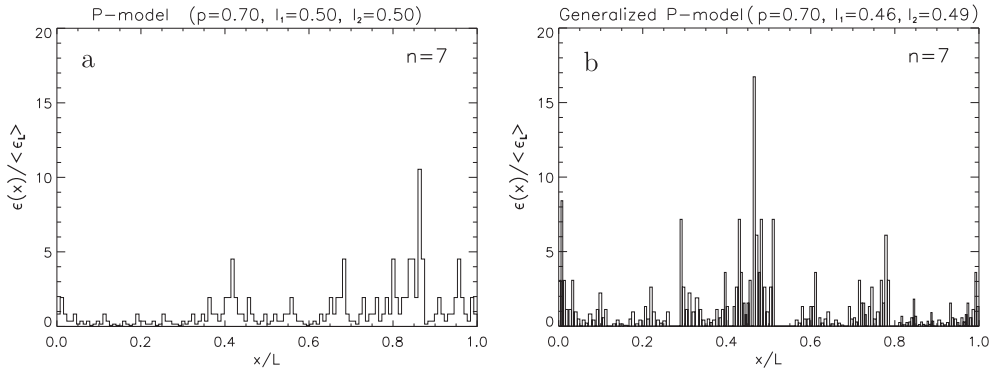

Fig. 3. The multifractal measure $\mu = \varepsilon / \langle \varepsilon_L \rangle$ on the unit interval for (a) the usual one-scale p-model and (b) the generalized two-scale cascade model. Intermittent pulses are stronger for the model with two different scaling parameters.

with a velocity amplitude $u(x)$ at a point x the transfer rate of this quantity $\varepsilon(x, l)$ is widely estimated by the third moment of increments of velocity fluctuations, e.g. (Frisch, 1995; Frisch et al., 1978)

$$\varepsilon(x, l) \sim \frac{|u(x + l) - u(x)|^3}{l}, \tag{2}$$

where $u(x)$ and $u(x + l)$ are velocity components parallel to the longitudinal direction separated from a position x by a distance l. Recently, limitations of this approximation are discussed and its hydromagnetic generalization for the Alfvénic fluctuations are considered (Marino et al., 2008; Sorriso-Valvo et al., 2007).

Now, we decompose the signal in segments of size l and then each segment is associated to an eddy. Therefore to each ith eddy of size l in the turbulence cascade we associate a probability measure defined by

$$p(x_i, l) \equiv \frac{\varepsilon(x_i, l)}{\sum_{i=1}^{N} \varepsilon(x_i, l)} = p_i(l). \tag{3}$$

This quantity can be interpreted as a probability that the energy is transferred to an eddy of size l. As is usual, at a given position $x = v_{\rm sw} t$, where $v_{\rm sw}$ is the average solar wind speed, the temporal scales measured in units of sampling time can be interpreted as the spatial scales $l = v_{\rm sw} \Delta t$ (Taylor's hypothesis).

2.4 Structure of Interplanetary Magnetic Fields

Let us take a stationary magnetic field $B(t)$ in the equatorial plane. We can again decompose this signal into time intervals of size Δt corresponding to the spatial scales $l = v_{\rm sw} \Delta t$. Then to each time interval one can associate a magnetic flux past the cross-section perpendicular to the plane during that time. In every considered year we use a discrete time series of daily averages, which is normalized so that we have $\langle B(t) \rangle = \frac{1}{N} \sum_{i=1}^{N} B(t_i) = 1$, where $i = 1, \ldots, N = 2^n$ (we take $n = 8$). Next, given this (normalized) time series $B(t_i)$, to each interval of temporal scale Δt (using $\Delta t = 2^k$, with $k = 0, 1, \ldots, n$) we associate some probability measure

$$p(x_j, l) \equiv \frac{1}{N} \sum_{i=1+(j-1)\Delta t}^{j\Delta t} B(t_i) = p_j(l), \tag{4}$$

where $j = 2^{n-k}$, i.e., calculated by using the successive average values $\langle B(t_i, \Delta t)\rangle$ of $B(t_i)$ between t_i and $t_i + \Delta t$ (Burlaga et al., 2006).

2.5 Scaling of Probability Measure and Generalized Dimensions

Now, for a continuous index $-\infty < q < \infty$ using a q-order total probability measure (Macek & Wawrzaszek, 2009)

$$I(q,l) \equiv \sum_{i=1}^{N} p_i^q(l) \tag{5}$$

and a q-order generalized information $H(q,l)$ (corresponding to Renyi's entropy) defined by Grassberger (1983)

$$H(q,l) \equiv -\log I(q,l) = -\log \sum_{i=1}^{N} p_i^q(l) \tag{6}$$

one obtains the usual q-order generalized dimensions (Hentschel & Procaccia, 1983) $D_q \equiv \tau(q) \ / \ (q-1)$, where

$$\tau(q) = \lim_{l \to 0} \frac{H(q,l)}{\log(1/l)} \ . \tag{7}$$

2.6 Generalized Measures and Multifractality

Using Equation (5), we also define a one-parameter q family of (normalized) generalized pseudoprobability measures (Chhabra et al., 1989; Chhabra & Jensen, 1989)

$$\mu_i(q,l) \equiv \frac{p_i^q(l)}{I(q,l)}. \tag{8}$$

Now, with an associated fractal dimension index $f_i(q,l) \equiv \log \mu_i(q,l) / \log l$ for a given q the multifractal singularity spectrum of dimensions is defined directly as the averages taken with respect to the measure $\mu(q,l)$ in Equation (8) denoted from here on by $\langle \ldots \rangle$ (skipping a subscript av)

$$f(q) \ \equiv \ \lim_{l \to 0} \sum_{i=1}^{N} \mu_i(q,l) \ f_i(q,l) = \langle f(q) \rangle \tag{9}$$

and the corresponding average value of the singularity strength is given by Chhabra & Jensen (1989)

$$\alpha(q) \ \equiv \ \lim_{l \to 0} \sum_{i=1}^{N} \mu_i(q,l) \ \alpha_i(l) = \langle \alpha(q) \rangle. \tag{10}$$

Hence by using a q-order mixed Shannon information entropy

$$S(q,l) = -\sum_{i=1}^{N} \mu_i(q,l) \log p_i(l) \tag{11}$$

we obtain the singularity strength as a function of q

$$\alpha(q) = \lim_{l \to 0} \frac{S(q,l)}{\log(1/l)} \ = \ \lim_{l \to 0} \frac{\langle \log p_i(l) \rangle}{\log(l)}, \tag{12}$$

Similarly, by using the q-order generalized Shannon entropy

$$K(q,l) = -\sum_{i=1}^{N} \mu_i(q,l) \log \mu_i(q,l) \tag{13}$$

we obtain directly the singularity spectrum as a function of q

$$f(q) = \lim_{l\to 0} \frac{K(q,l)}{\log(1/l)} \;=\; \lim_{l\to 0} \frac{\langle \log \mu_i(q,l) \rangle}{\log(l)}. \tag{14}$$

One can easily verify that the multifractal singularity spectrum $f(\alpha)$ as a function of α satisfies the following Legendre transformation (Halsey et al., 1986; Jensen et al., 1987):

$$\alpha(q) \;=\; \frac{\mathrm{d}\,\tau(q)}{\mathrm{d}q}, \qquad f(\alpha) \;=\; q\alpha(q) - \tau(q). \tag{15}$$

2.7 Two-scale weighted Cantor set

Let us now consider the generalized weighted Cantor set, as shown in Figure 2, where the probability of providing energy for one eddy of size l_1 is p (say, $p \leq 1/2$), and for the other eddy of size l_2 is $1-p$. At each stage of construction of this generalized Cantor set we basically have two rescaling parameters l_1 and l_2, where $l_1 + l_2 \leq L = 1$ (normalized) and two different probability measure $p_1 = p$ and $p_2 = 1-p$. To obtain the generalized dimensions $D_q \equiv \tau(q)/(q-1)$ for this multifractal set we use the following partition function (a generator) at the n-th level of construction (Halsey et al., 1986; Hentschel & Procaccia, 1983)

$$\Gamma_n^q(l_1, l_2, p) = \left(\frac{p^q}{l_1^{\tau(q)}} + \frac{(1-p)^q}{l_2^{\tau(q)}} \right)^n \;=\; 1. \tag{16}$$

We see that after n iterations, $\tau(q)$ does not depend on n, we have $\binom{n}{k}$ intervals of width $l = l_1^k l_2^{n-k}$, where $k = 1, \ldots, n$, visited with various probabilities. The resulting set of 2^n closed intervals (more and more narrow segments of various widths and probabilities) for $n \to \infty$ becomes the weighted two-scale Cantor set.
For any q in Equation (16) one obtains $D_q = \tau(q)/(q-1)$ by solving numerically the following transcendental equation (e.g., Ott, 1993)

$$\frac{p^q}{l_1^{\tau(q)}} + \frac{(1-p)^q}{l_2^{\tau(q)}} = 1. \tag{17}$$

When both scales are equal $l_1 = l_2 = \lambda$, Equation (17) can be solved explicitly to give the formula for the generalized dimensions (Macek, 2006a; 2007)

$$\tau(q) \equiv (q-1)D_q = \frac{\ln[p^q + (1-p)^q]}{\ln \lambda}. \tag{18}$$

For space filling turbulence ($\lambda = 1/2$) one recovers the formula for the multifractal cascade of the standard $p-$model for fully developed turbulence (Meneveau & Sreenivasan, 1987), which obviously corresponds to the weighted one-scale Cantor set (Hentschel & Procaccia, 1983), (cf. Macek, 2002, Figure 3) and (Macek et al., 2006, Figure 3 (b)).

2.8 Multifractal Formalism

Theory of multifractals allows us an intuitive understanding of multiplicative processes and of the intermittent distributions of various characteristics of turbulence, see (Wawrzaszek & Macek, 2010). As an extension of fractals, multifractals could be seen as objects that demonstrate various self-similarities at various scales. Consequently, the multifractals are described by an infinite number of the generalized dimensions, D_q, as depicted in Figure 4a and by the multifractal spectrum $f(\alpha)$ sketched in Figure 4b (Halsey et al., 1986). The generalized dimensions D_q are calculated as a function of a continuous index q (Grassberger, 1983; Grassberger & Procaccia, 1983; Halsey et al., 1986; Hentschel & Procaccia, 1983). This parameter q, where $-\infty < q < \infty$, can be compared to a microscope for exploring different regions of the singular measurements. In the case of turbulence cascade the generalized dimensions are related to inhomogeneity with which the energy is distributed between different eddies (Meneveau & Sreenivasan, 1991). In this way they provide information about dynamics of multiplicative process of cascading eddies. Here high positive values of q emphasize regions of intense energy transfer rate, while negative values of q accentuate low-transfer rate regions. Similarly, high positive values of q emphasize regions of intense magnetic fluctuations larger than the average, while negative values of q accentuate fluctuations lower than the average (Burlaga, 1995).

An alternative description can be formulated by using the singularity spectrum $f(\alpha)$ as a function of a singularity strength α, which quantify multifractality of a given system (e.g., Ott, 1993). This function describes singularities occurring in considered probability measure attributed to different regions of the phase space of a given dynamical system. Admittedly, both functions $f(\alpha)$ and D_q have the same information about multifractality. However, the singularity multifractal spectrum is easier to interpret theoretically by comparing the experimental results with the models under study.

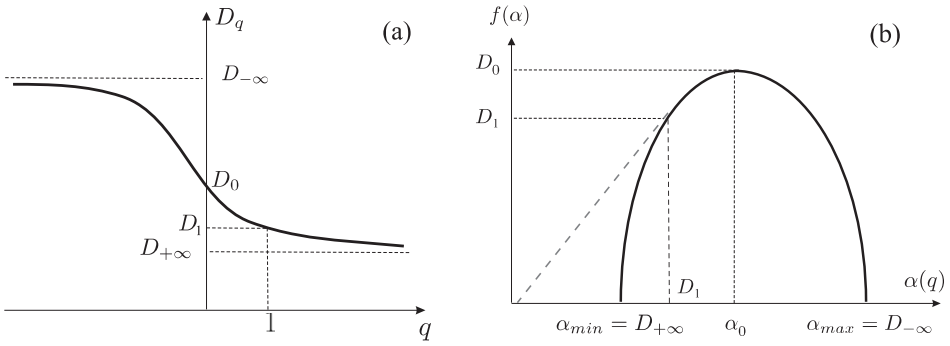

Fig. 4. (a) The generalized dimensions D_q as a function of any real q, $-\infty < q < +\infty$, and (b) the singularity multifractal spectrum $f(\alpha)$ versus the singularity strength α with some general properties: (1) the maximum value of $f(\alpha)$ is D_0; (2) $f(D_1) = D_1$; and (3) the line joining the origin to the point on the $f(\alpha)$ curve, where $\alpha = D_1$ is tangent to the curve (Ott, 1993).

2.9 Degree of Multifractality and Asymmetry

The difference of the maximum and minimum dimension (the least dense and most dense points in the phase space) is given by

$$\Delta \equiv \alpha_{\max} - \alpha_{\min} = D_{-\infty} - D_{\infty} = \left| \frac{\log(1-p)}{\log l_2} - \frac{\log(p)}{\log l_1} \right| \tag{19}$$

as the degree of multifractality, see (e.g., Macek, 2006a; 2007). In the limit $p \to 0$ this difference rises to infinity. The degree of multifractality Δ is simply related to the deviation from a simple self-similarity. That is why Δ is also a measure of intermittency, which is in contrast to self-similarity (Frisch, 1995, ch. 8).

In the case of a symmetric spectrum using Equation (18) the degree of multifractality is

$$\Delta = D_{-\infty} - D_{+\infty} = \ln(1/p - 1)/\ln(1/\lambda) \tag{20}$$

In particular, the usual middle one-third Cantor set without any multifractality is recovered with $p = 1/2$ and $\lambda = 1/3$.

Moreover, using the value of the strength of singularity α_0 at which the singularity spectrum has its maximum $f(\alpha_0) = 1$ we define a measure of asymmetry by

$$A \equiv \frac{\alpha_0 - \alpha_{\min}}{\alpha_{\max} - \alpha_0}. \tag{21}$$

3. Solar Wind Data

We have analyzed time series of plasma velocity and interplanetary magnetic field strength measured during space missions onboard various spacecraft, such as Helios, ACE, Ulysses, and Voyager, exploring different regions of the heliosphere during solar minimum and solar maximum.

3.1 Solar Wind Velocity Fluctuations

3.1.1 Inner Heliosphere

Macek (2007) has analyzed the Helios 2 data using plasma parameters measured *in situ* in the inner heliosphere with sampling time of 40.5 s (Schwenn, 1990). The X-velocity (mainly radial) component of the plasma flow, v_x, (4514 points) has already been investigated by Macek (1998; 2002; 2003) and Macek & Redaelli (2000). The Alfvénic fluctuations with longer (two-day) samples have been studied by Macek (2006a; 2007) and Macek et al. (2005; 2006). To study turbulence cascade, Macek & Szczepaniak (2008) have even selected four-day time intervals of v_x samples in 1976 (solar minimum) for both slow and fast solar wind streams measured at various distances from the Sun. The results for data obtained by ACE in the ecliptic plane near the libration point $L1$, i.e., approximately at a distance of $R = 1$ AU from the Sun and dependence on solar cycle have been discussed by Szczepaniak & Macek (2008). They have studied the multifractal measure obtained using $N = 2^n$, with $n = 18$, data points for (a) solar minimum (2006) and (b) solar maximum (2001), correspondingly. For example, the obtained probability density functions of fluctuations of the solar wind velocity is shown in Figure 5 taken from (Szczepaniak & Macek, 2008).

In addition, Macek et al. (2009) have analyzed time series of velocities of the solar wind measured by ACE separately for both slow and fast solar wind streams during solar minimum (2006) and maximum (2001). They have selected five-day time intervals of v_x samples, each of 6750 data points, interpolated with sampling time of 64 s, for both slow and fast solar wind

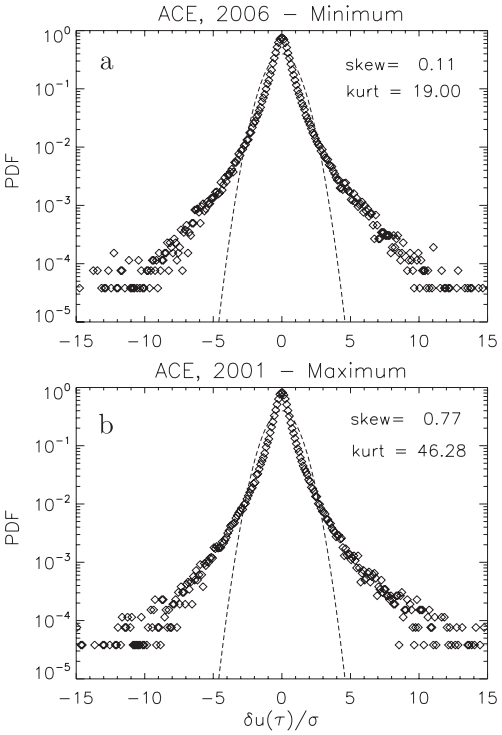

Fig. 5. Probability density functions of fluctuations of the solar wind radial velocity for (a) solar minimum (2006) and (b) solar maximum (2001), correspondingly, as compared with the normal distribution (dashed lines).

streams during solar minimum (2006) and maximum (2001). In Figure 6 taken from (Macek et al., 2009) we show the time trace of the multifractal measure $p(t_i, \Delta t) = \varepsilon(t_i, \Delta t) \; / \; \sum \varepsilon(t_i, \Delta t)$ given by Eqs. (2) and (3) and obtained using data of the velocity components $u = v_x$ (in time domain) as measured by ACE at 1 AU for the slow (a) and (c) and fast (b) and (d) solar wind during solar minimum (2006) and maximum (2001), correspondingly. One can notice that intermittent pulses are somewhat stronger for data at solar maximum. This results in fatter tails of the probability distribution functions as shown in Figure 5, for solar maximum and minimum with large deviations from the normal distribution (dashed lines).

3.1.2 Outer Heliosphere

Macek & Wawrzaszek (2009) have tested asymmetry of the multifractal scaling for the wealth of data provided by another space mission. Namely, they have analyzed time series of velocities of the solar wind measured by Voyager 2 at various distances from the Sun, 2.5, 25, and 50 AU. selecting long (13-day) time intervals of v_x samples, each of 2^{11} data points, interpolated with sampling time of 192 s for both slow and fast solar wind streams during the following solar minima: 1978, 1987–1988, and 1996–1997. The same analysis has been repeated for the Voyager 2 data for the slow solar wind during the solar maxima: 1981, 1989, 2001, at 10, 30,

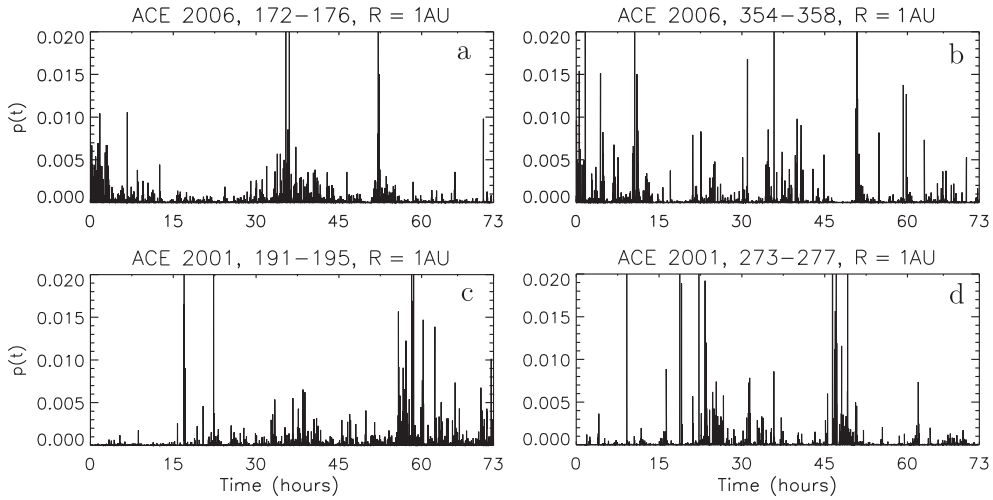

Fig. 6. The time trace of the normalized transfer rate of the energy flux $p(t_i, \Delta t) = \varepsilon(t_i, \Delta t) \; / \; \sum \varepsilon(t_i, \Delta t)$ obtained using data of the v_x velocity components measured by ACE at 1 AU for the slow (a) and (c) and fast (b) and (d) solar wind during solar minimum (2006) and maximum (2001), correspondingly.

and 65 AU, correspondingly. This has allowed us to investigate the dependence of the multifractal spectra on the phase of the solar cycle (Macek & Wawrzaszek, 2011b).

3.1.3 Out-of Ecliptic

It is worth noting that Ulysses' periodic (6.2 years) orbit with perihelion at 1.3 AU and aphelion at 5.4 AU and latitudinal excursion of $\pm 82^\circ$ gives us a new possibility enabling to study both latitudinal and radial dependence of the solar wind (Horbury et al., 1996; Smith et al., 1995).

Wawrzaszek & Macek (2010) have determined multifractal characteristics of turbulence scaling such as the degree of multifractality and asymmetry of the multifractal singularity spectrum for the data provided by Ulysses space mission. They have used plasma flow measurements as obtained from the SWOOPS instrument (Solar Wind Observations Over the Poles of the Sun). Namely, they have analyzed time series of velocities of the solar wind measured by Ulysses out of the ecliptic plane at different heliographic latitudes ($+32^\circ \div +40^\circ$, $+47^\circ \div +48^\circ$, $+74^\circ \div +78^\circ$, $-40^\circ \div -47^\circ$, $-50^\circ \div -56^\circ$, $-69^\circ \div -71^\circ$) and heliocentric distances of $R = 1.4 - 5.0$ AU from the Sun. selecting twelve-days time intervals of v_x samples, each of 4096 data points, with sampling time of 242 s $\approx$4 min, for solar wind streams during solar minimum (1994 - 1997, 2006 - 2007).

3.2 Magnetic Field Strength Fluctuations

Macek & Wawrzaszek (2011a) have tested the multifractal scaling of the interplanetary magnetic field strengths, B, for the wealth of data provided by ACE mission, located in the ecliptic plane near the libration point $L1$, i.e., approximately at a distance of $R = 1$ AU from the Sun. In case of ACE the sampling time resolution of 16 s for the magnetic field is much better than

that for the Voyager data, which allow us to investigate the scaling on small scales of the order of minutes.
The calculated energy spectral density as a function of frequency for the data set of the magnetic field strengths $|B|$ consisting of about 2×10^6 measurements for (a) the whole year 2006 during solar minimum and (b) the whole year 2001 during solar maximum is illustrated in Figure 1 of the paper by Macek & Wawrzaszek (2011a). It has been shown that the spectrum density is roughly consistent with this well-known power-law dependence $E(f) \propto f^{-5/3}$ at wide range of frequency, f, suggesting a self-similar fractal turbulence model often used for looking at scaling properties of plasma fluctuations (e.g., Burlaga & Klein, 1986). However, it is clear that the spectrum alone, which is based on a second moment (or a variance), cannot fully describe fluctuations in the solar wind turbulence (cf. Alexandrova et al., 2007). Admittedly, intermittency, which is deviation from self-similarity (e.g., Frisch, 1995), usually results in non-Gaussian probability distribution functions. However, the multifractal powerful method generalizes these scaling properties by considering not only various moments of the magnetic field, but the whole spectrum of scaling indices (Halsey et al., 1986).
Therefore, Macek & Wawrzaszek (2011a) have further analyzed time series of the magnetic field of the solar wind on both small and large scales using multifractal methods. To investigate scaling properties in fuller detail, using basic 64-s sampling time for small scales, they have selected long time intervals of $|B|$ of interpolated samples, each of 2^{18} data points, from day 1 to 194. Similarly, for large scales they have used daily averages of samples from day 1 to 256 of 2^8 data points. The data for both small and large scale fluctuations during solar minimum (2006) and maximum (2001) are shown in Figure 2 of (Macek & Wawrzaszek, 2011a).

4. Results and Discussion

4.1 Multifractal Model for Plasma Turbulence

For a given q, we calculate the generalized q-order total probability measure $I(q,l)$ of Equation (5) as a function of various scales l that cover turbulence cascade (cf. Macek & Szczepaniak, 2008, Equation (2)). On a small scale l in the scaling region one should have, according to Equations (5) to (7), $I(q,l) \propto l^{\tau(q)}$, where $\tau(q)$ is an approximation of the ideal limit $l \to 0$ solution of Equation (7) (e.g., Macek et al., 2005, Equation (1)). Equivalently, writing $I(q,l) = \sum p_i (p_i)^{q-1}$ as a usual weighted average of $\langle (p_i)^{q-1} \rangle_{\mathrm{av}}$, one can associate bulk with the generalized average probability per cascading eddies

$$\bar{\mu}(q,l) \equiv \sqrt[q-1]{\langle (p_i)^{q-1} \rangle_{\mathrm{av}}}, \tag{22}$$

and identify D_q as a scaling of bulk with size l,

$$\bar{\mu}(q,l) \propto l^{D_q}. \tag{23}$$

Hence, the slopes of the logarithm of $\bar{\mu}(q,l)$ of Equation (23) versus $\log l$ (normalized) provides

$$D_q(l) = \frac{\log \bar{\mu}(q,l)}{\log l}. \tag{24}$$

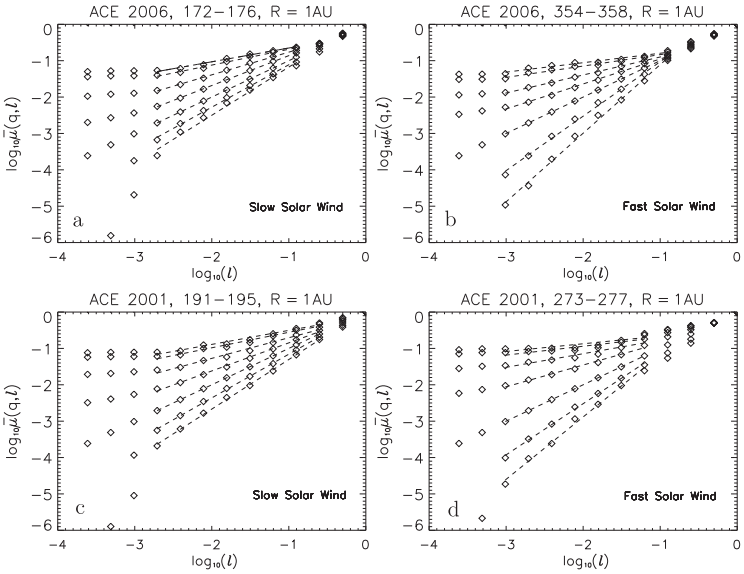

Fig. 7. Plots of the generalized average probability of cascading eddies $\log_{10} \bar{\mu}(q,l)$ versus $\log_{10} l$ for the following values of q: 6, 4, 2, 1, 0, -1, -2, measured by ACE at 1 AU (diamonds) for the slow (a) and (c) and fast (b) and (d) solar wind during solar minimum (2006) and maximum (2001), correspondingly.

4.1.1 Inner Heliosphere

In Figure 7 we have depicted some of the values of the generalized average probability, $\log \bar{\mu}(q,l)$, for the following values of q: 6, 4, 2, 1, 0, -1, -2. These results are obtained using data of the v_x velocity components measured by ACE at 1 AU (diamonds) for the slow (a) and (c) and fast (b) and (d) solar wind during solar minimum (2006) and maximum (2001), correspondingly. The generalized dimensions D_q as a function of q are shown in Figure 8. The values of D_q given in Equation (24), are calculated using the radial velocity components $u = v_x$, cf. (Macek et al., 2005, Figure 3),

In addition, in Figures 9 and 10 we see the generalized average logarithmic probability and pseudoprobability measures of cascading eddies $\langle \log_{10} p_i(l) \rangle$ and $\langle \log_{10} \mu_i(q,l) \rangle$ versus $\log_{10} l$, as given in Equations (3) and (8). The obtained results for the singularity spectra $f(\alpha)$ as a function of α are shown in Figure 11 for the slow (a) and (c), and fast (b) and (d) solar wind streams at solar minimum and maximum, correspondingly. Both values of D_q and $f(\alpha)$ for one-dimensional turbulence have been computed directly from the data, by using the experimental velocity components.

For $q \geq 0$ these results agree with the usual one-scale p-model fitted to the dimension spectra as obtained analytically using $l_1 = l_2 = 0.5$ in Equation (18) and the corresponding value of the parameter $p \simeq 0.21$ and 0.20, 0.15 and 0.12 for the slow (a) and (c), and fast (b) and (d) solar wind streams at solar minimum and maximum, correspondingly, as shown by dashed lines. On the contrary, for $q < 0$ the p-model cannot describe the observational results (Marsch et al., 1996). Here we show that the experimental values are consistent also with the generalized dimensions obtained numerically from Eqs. (22-24) for the weighted two-scale Cantor set using

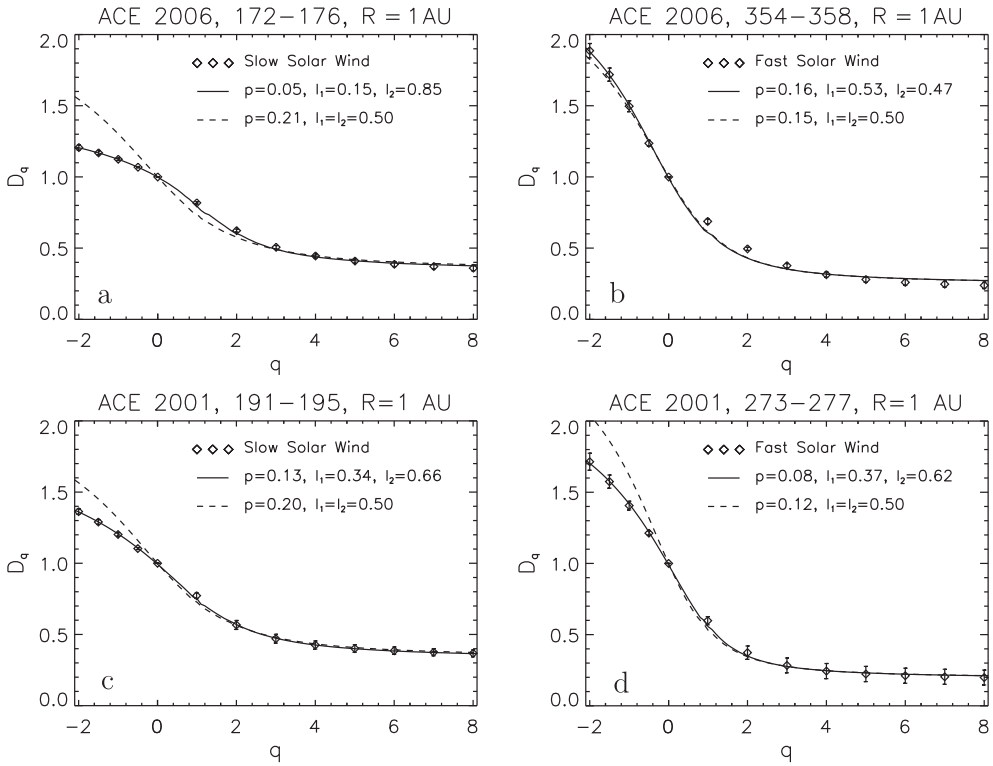

Fig. 8. The generalized dimensions D_q as a function of q. The values obtained for one-dimensional turbulence are calculated for the usual one-scale (dashed lines) p-model and the generalized two-scale (continuous lines) model with parameters fitted to the multifractal measure $\mu(q,l)$ obtained using data measured by ACE at 1 AU (diamonds) for the slow (a) and (c) and fast (b) and (d) solar wind during solar minimum (2006) and maximum (2001), correspondingly.

an asymmetric scaling, i.e., using unequal scales $l_1 \neq l_2$, as is shown in Figure 8 (a), (b), (c), and (d) by continuous lines. We also confirm the universal shape of the multifractal spectrum, Figure 11. In our view, this obtained shape of the multifractal spectrum results not only from the nonuniform probability of the energy transfer rate but mainly from the multiscale nature of the cascade.

It is well known that the fast wind is associated with coronal holes, while the slow wind mainly originates from the equatorial regions of the Sun. Consequently, the structure of the flow differs significantly for the slow and fast streams. Hence the fast wind is considered to be relatively uniform and stable, while the slow wind is more turbulent and quite variable in velocities, possibly owing to a strong velocity shear (Goldstein et al., 1995). We see from Table 1 that the degree of multifractality Δ and asymmetry A of the solar wind in the inner heliosphere are different for slow ($\Delta = 1.2 - 1.6$) and fast ($\Delta = 2.3 - 2.6$) streams; the velocity fluctuations in the fast streams seem to be more multifractal than those for the slow solar wind (the generalized dimensions vary more with the index q). On the other hand, it seems that in

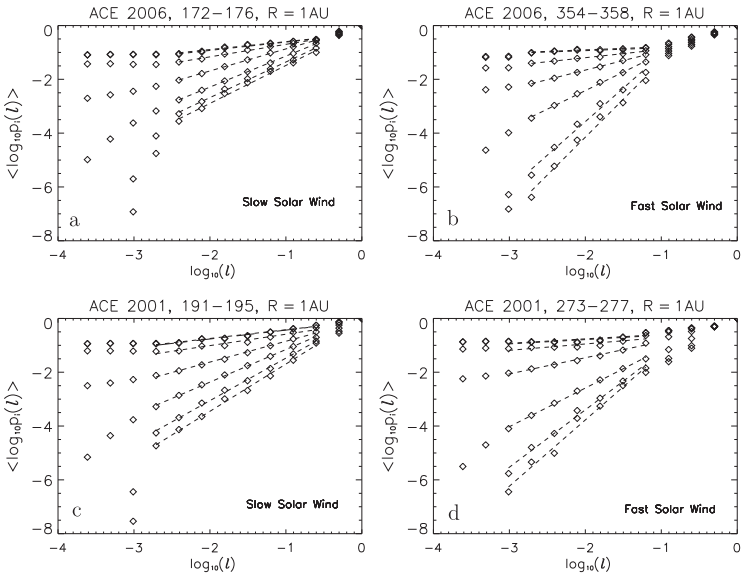

Fig. 9. Plots of the generalized average logarithmic probability of cascading eddies $\langle \log_{10} p_i(l) \rangle$ versus $\log_{10} l$. for the following values of q: 2, 1, 0, -1, -2, measured by ACE at 1 AU (diamonds) for the slow (a) and (c) and fast (b) and (d) solar wind during solar minimum (2006) and maximum (2001), correspondingly.

Table 1. Degree of multifractality Δ and asymmetry A for solar wind data in the inner heliosphere

	Slow Solar Wind	Fast Solar Wind
Solar Min.	$\Delta = 1.22, A = 2.21$	$\Delta = 2.56, A = 0.95$
Solar Max.	$\Delta = 1.60, A = 1.33$	$\Delta = 2.31, A = 1.25$

the slow streams the scaling is more asymmetric than that for the fast wind. In our view this could possibly reflect the large-scale scale velocity structure. Further, the degree of asymmetry of the dimension spectra for the slow wind is rather anticorrelated with the phase of the solar magnetic activity and only weakly correlated for the fast wind: A decreases from 2.2 to 1.3 and only the fast wind during solar minimum exhibits roughly symmetric scaling, $A \sim 1$, i.e., one-scale Cantor set model applies.

4.1.2 Outer Heliosphere

These results are obtained using data of the v_x velocity components measured by Voyager 2 during solar minimum (1978, 1987–1988, 1996–1997) at various distance from the Sun: 2.5, 25, and 50 AU. In this way, the singularity spectra $f(\alpha)$ are obtained directly from the data as a function of α as given by Equations (12) and (14) and the results are presented in Figure 12 (diamonds) for the slow (a), (c), and (e) and fast (b), (d), and (f) solar wind, correspondingly.

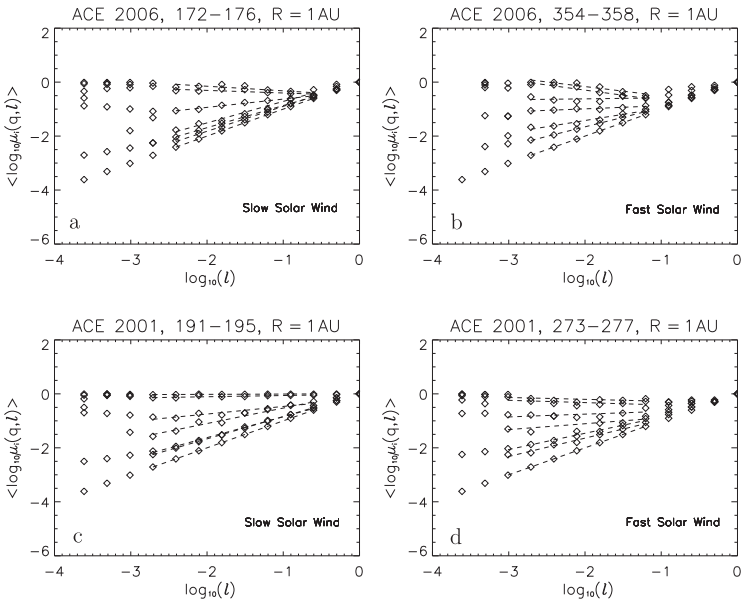

Fig. 10. Plots of the generalized average logarithmic pseudoprobability measure of cascading eddies $\langle \log_{10} \mu_i(q,l) \rangle$ versus $\log_{10} l$ for the following values of q: 2, 1, 0, -1, -2, measured by ACE at 1 AU (diamonds) for the slow (a) and (c) and fast (b) and (d) solar wind during solar minimum (2006) and maximum (2001), correspondingly.

We see from Table 2 that the obtained values of Δ obtained from Equation (19) for the solar wind in the outer heliosphere are somewhat different for slow and fast streams. For the fast wind (not very far away from the Sun) D_q fells more steeply with q than for the slow wind, and therefore one can say that the degree of multifractality is larger for the fast wind.

4.1.3 Out-off Ecliptic

Wawrzaszek & Macek (2010) have observed a latitudinal dependence of the multifractal characteristics of turbulence. The calculated degree of multifractality and asymmetry as a function on heliographic latitude for the fast solar wind are summarized in Figure 13 and 14a with some specific values listed in Table 3 (the case of the slow wind is denoted by an asterisk). We see from Table 3 that the degree of multifractality Δ and asymmetry A of the dimension spectra of

Table 2. Degree of multifractality Δ and asymmetry A for solar wind data in the outer heliosphere during solar minimum.

Heliospheric distance (year)	Slow Solar Wind	Fast Solar Wind
2.5 AU (1978)	$\Delta = 1.95, A = 0.91$	$\Delta = 2.12, A = 1.54$
25 AU (1987-1988)	$\Delta = 2.02, A = 0.98$	$\Delta = 2.93, A = 0.66$
50 AU (1996-1997)	$\Delta = 2.10, A = 1.14$	$\Delta = 1.94, A = 0.95$

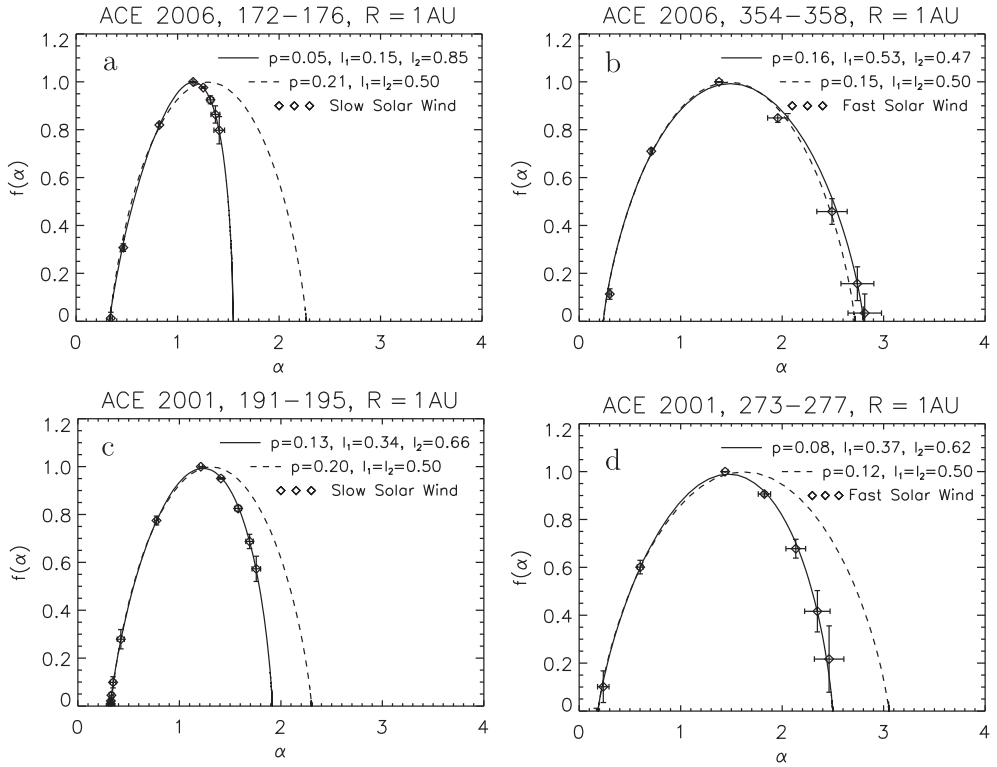

Fig. 11. The corresponding singularity spectrum $f(\alpha)$ as a function of α.

the fast solar wind out of the ecliptic plane are similar for positive and the corresponding negative latitudes. Therefore, it seems that the values of these multifractal characteristics exhibits some symmetry with respect to the ecliptic plane. In particular, in a region from 50° to 70° we observe a minimum of the degree of multifractality (intermittency). This could be related to interactions between fast and slow streams, which usually can still take place at latitudes from 30° to 50°. Another possibility is appearance of first new solar spots for a subsequent solar cycle at some intermediate latitudes. At polar regions, where the pure fast streams are present, the degree of multifractality rises again. It is interesting that a similar behavior of flatness, which is another measure of intermittency, has been observed at high latitudes by using the magnetic data (Yordanova et al., 2009).

Further, the degree of multifractality and asymmetry seem to be somewhat correlated. We see that when latitudes change from $+32^\circ \div +40^\circ$ to $-50^\circ \div -56^\circ$ then Δ decreases from 1.50 to 1.27, and the value of A changes only slightly from 1.10 to 1.07. Only at very high polar regions larger than 70° this correlation ceases. Moreover, the scaling of the fast streams from the polar region of the Sun exhibit more multifractal and asymmetric character, $\Delta = 1.80$, $A = 0.80$, than that for the slow wind from the equatorial region, $\Delta = 1.52$, $A = 1.14$ (in both cases we have relatively large errors of these parameters). In Figure 14b we show how the parameters of the two-scale Cantor set model p and l_1 (during solar minimum) depend on the

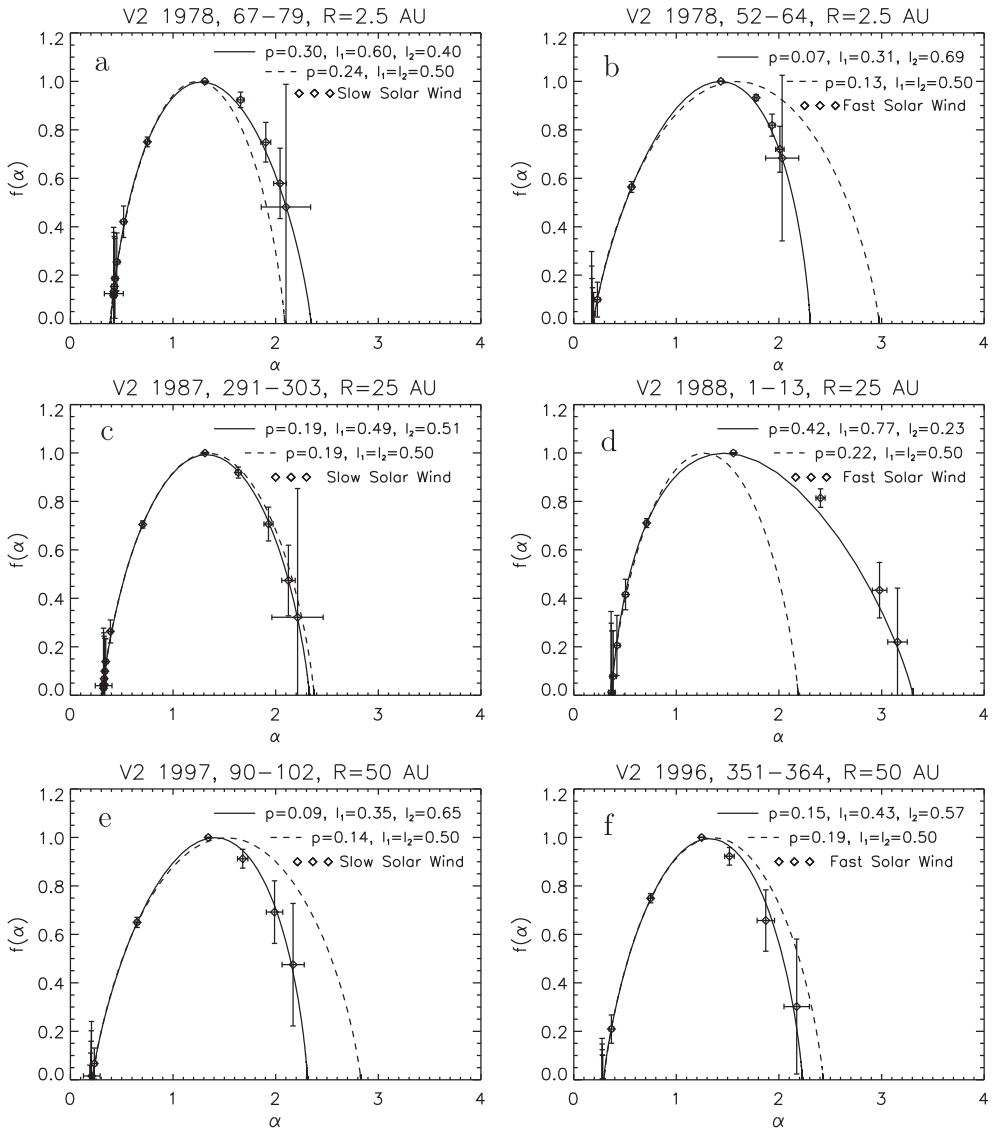

Fig. 12. The singularity spectrum $f(\alpha)$ calculated for the one-scale p-model (dashed lines) and the generalized two-scale (continuous lines) models with parameters fitted to the multifractal measure $\mu(q,l)$ using data measured by Voyager 2 during solar minimum (1978, 1987–1988, 1996–1997) at 2.5, 25, and 50 AU (diamonds) for the slow (a, c, e) and fast (b, d, f) solar wind, correspondingly.

heliographic latitudes, rising at $\sim 50^\circ$ and again above $\sim 70^\circ$. It is clear that both parameters seem to be correlated.

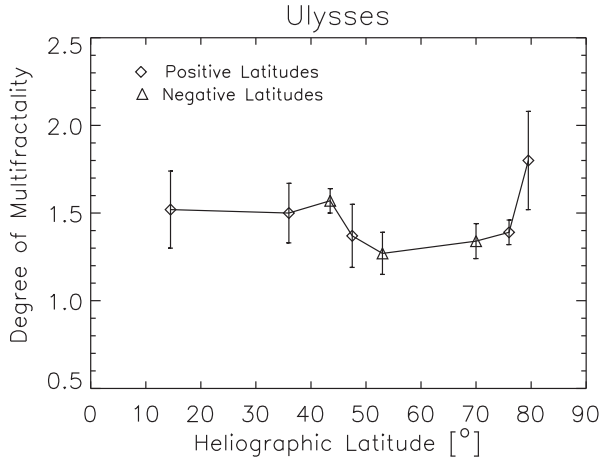

Fig. 13. Degree of multifractality Δ (continuous line) for the slow (at 15°) and fast (above 15°) solar wind during solar minimum (1994 - 1996, 2006 - 2007) in dependence on heliographic latitude below (triangles) and above (diamonds) the ecliptic.

Table 3. Degree of Multifractality Δ and Asymmetry A for the Energy Transfer Rate in the Out of Ecliptic Plane.

Heliographic Latitude	**Heliocentric Distance**	**Multifractality Δ**	**Asymmetry A**
$+14^\circ \div +15^\circ$ (1997)*	4.9 AU	1.52 ± 0.22	1.14 ± 0.30
$+32^\circ \div +40^\circ$ (1995)	1.4 AU	1.50 ± 0.17	1.10 ± 0.20
$+47^\circ \div +48^\circ$ (1996)	3.3 AU	1.37 ± 0.18	1.21 ± 0.32
$+74^\circ \div +78^\circ$ (1995)	$1.8 - 1.9$ AU	1.39 ± 0.07	1.17 ± 0.12
$+79^\circ \div +80^\circ$ (1995)	$1.9 - 2.0$ AU	1.80 ± 0.28	0.80 ± 0.29
$-40^\circ \div -47^\circ$ (2007)	1.6 AU	1.57 ± 0.07	1.53 ± 0.20
$-50^\circ \div -56^\circ$ (1994)	$1.6 - 1.7$ AU	1.27 ± 0.12	1.07 ± 0.20
$-69^\circ \div -71^\circ$ (2006)	$2.8 - 2.9$ AU	1.34 ± 0.10	1.36 ± 0.25

Let us now compare the results obtained out-off ecliptic with those obtained at the ecliptic plane using the generalized two-scale cascade model. First, as seen from Table 1, our analysis of the data obtained onboard ACE spacecraft at the Earth's orbit, especially in the fast solar wind, indicates multifractal structure with the degree of multifractality of $\Delta = 2.56 \pm 0.16$ and the degree of asymmetry $A = 0.95 \pm 0.11$ during solar minimum (Macek et al., 2009). Similar values are obtained by Voyager spacecraft, e.g. Table 2, at distance of 2.5 AU we have $\Delta = 2.12 \pm 0.14$ and $A = 1.54 \pm 0.24$, and in the outer heliosphere at 25 AU we have also large values $\Delta = 2.93 \pm 0.10$ and rather asymmetric spectrum $A = 0.66 \pm 0.11$ (Macek & Wawrzaszek, 2009). We see that at high latitudes during solar minimum in the fast solar

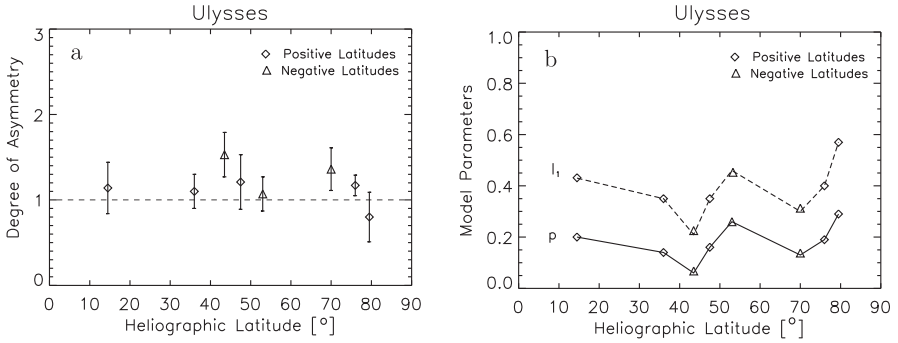

Fig. 14. (a) Degree of asymmetry A and (b) change of two-scale model parameters p (continuous line) and l_1 (dashed line) in dependence on heliographic latitude during solar minimum (1994 - 1996, 2006 - 2007).

wind, Table 3, we observe somewhat smaller degree of multifractality and intermittency as compared with those at the ecliptic, Table 2.
These results are consistent with previous results confirming that slow wind intermittency is higher than that for the fast wind (e.g., Sorriso-Valvo et al., 1999), and that intermittency in the fast wind increases with the heliocentric distance, including high latitudes (e.g., Bruno et al., 2003; 2001). In addition, symmetric multifractal singularity spectra are observed at high latitudes, in contrast to often significant asymmetry of the multifractal singularity spectrum at the ecliptic wind. This demonstrate that solar wind turbulence may exhibit somewhat different scaling at various latitudes resulting from different dynamics of the ecliptic and polar winds. Notwithstanding of the complexity of solar wind fluctuations it appears that the standard one-scale p model can roughly describe these nonlinear fluctuations out of the ecliptic, hopefully also in the polar regions. However, the generalized two-scale Cantor set model is necessary for describing scaling of solar wind intermittent turbulence near the ecliptic.
Summarizing, we see that the multifractal spectrum of the solar wind is only roughly consistent with that for the multifractal measure of the self-similar weighted symmetric one-scale weighted Cantor set only for $q \geq 0$. On the other hand, this spectrum is in a very good agreement with two-scale asymmetric weighted Cantor set schematically shown in Figure 2 for both positive and negative q. Obviously, taking two different scales for eddies in the cascade, one obtains a more general situation than in the usual p-model for fully developed turbulence (Meneveau & Sreenivasan, 1987), especially for an asymmetric scaling, $l_1 \neq l_2$.

4.2 Multifractal Model for Magnetic Turbulence

In the inertial region the q-order total probability measure, the partition function in Equation (4), should scale as

$$\sum p_j^q(l) \sim l^{\tau(q)}, \tag{25}$$

with $\tau(q)$ given in Equation (7). In this case Burlaga (1995) has shown that the average value of the qth moment of the magnetic field strength B at various scales $l = v_{\rm sw}\Delta t$ scales as

$$\langle B^q(l) \rangle \sim l^{\gamma(q)}, \tag{26}$$

with the similar exponent $\gamma(q) = (q-1)(D_q - 1)$.
For a given q, using the slopes $s(q)$ of $\log_{10}\langle B^q \rangle$ versus $\log_{10}\tau$ in the inertial range one can obtain the values of D_q as a function of q according to Equation (26). Equivalently, as discussed in Subsection 2.8, the multifractal spectrum $f(\alpha)$ as a function of scaling indices α indicates universal multifractal scaling behavior.

4.2.1 Inner Heliosphere

Macek & Wawrzaszek (2011a) have shown that the degree of multifractality for magnetic field fluctuations of the solar wind at ∼1 AU for large scales from 2 to 16 days is greater than that for the small scales from 2 min. to 18 h. In particular, they have demonstrated that on small scales the multifractal scaling is strongly asymmetric in contrast to a rather symmetric spectrum on the large scales, where the evolution of the multifractality with the solar cycle is also observed.

4.2.2 Outer Heliosphere and the Heliosheath

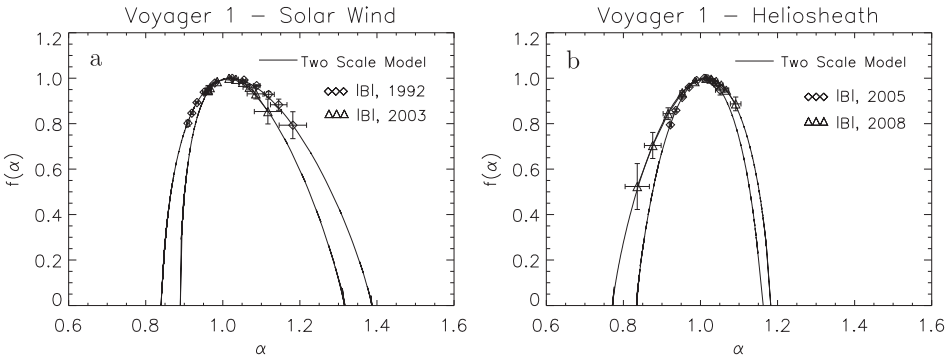

Fig. 15. The multifractal singularity spectrum of the magnetic fields observed by Voyager 1 (a) in the solar wind near 50 and 90 AU (1992, diamonds, and 2003, triangles) and (b) in the heliosheath near 95 and 105 AU (2005, diamonds, and 2008, triangles) together with a fit to the two-scale model (solid curve), suggesting change of the symmetry of the spectrum at the termination shock.

Further, the results for the multifractal spectrum $f(\alpha)$ obtained using the Voyager 1 data of the solar wind magnetic fields in the distant heliosphere beyond the planets, at 50 AU (1992, diamonds) and 90 AU (2003, triangles), and after crossing the heliospheric shock, at 95 AU (2005, diamonds) and 105 AU (2008, triangles), are presented in Figures 15 (a) and (b), correspondingly, taken from (Macek et al., 2011). It is worth noting a change of the symmetry of the spectrum at the shock relative to its maximum at a critical singularity strength $\alpha = 1$. Because the density of the measure $\varepsilon \propto \tau^{\alpha-1}$, this is related to changing properties of the magnetic field density ε at the termination shock. Consequently, a concentration of magnetic fields shrinks resulting in thinner flux tubes or stronger current concentration in the heliosheath.
Macek et al. (2011) were also looking for the degree of multifractality Δ in the heliosphere as a function of the heliospheric distances during solar minimum (MIN), solar maximum (MAX), declining (DEC) and rising (RIS) phases of solar cycles. The obtained values of Δ roughly follow the fitted periodically decreasing function of time (in years, dotted), $20.27 - 0.00992t +$

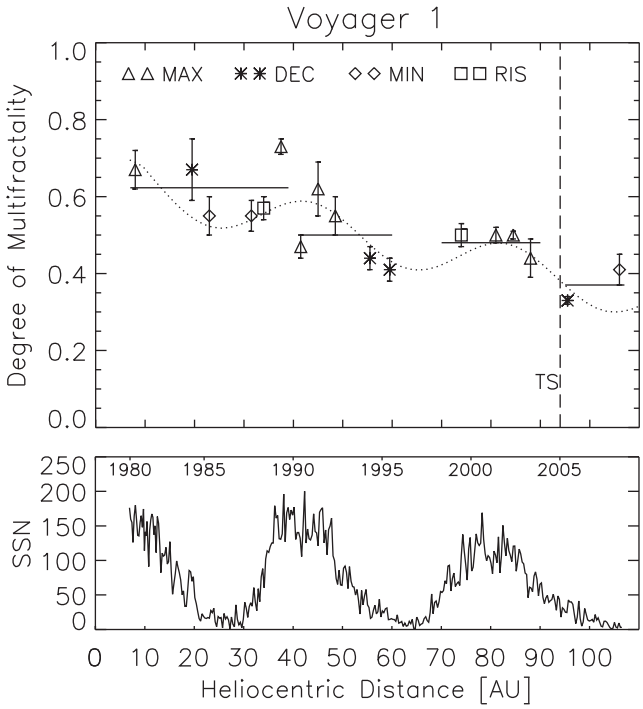

Fig. 16. The degree of multifractality Δ in the heliosphere versus the heliospheric distances compared to a periodically decreasing function (dotted) during solar minimum (MIN) and solar maximum (MAX), declining (DEC) and rising (RIS) phases of solar cycles, with the corresponding averages shown by continuous lines. The crossing of the termination shock (TS) by Voyager 1 is marked by a vertical dashed line. Below is shown the Sunspot Number (SSN) during years 1980–2008.

$0.06\sin((t-1980)/(2\pi(11))+\pi/2)$, with the corresponding averages shown by continuous lines in Figure 16 taken from (Macek et al., 2011). The crossing of the termination shock (TS) by Voyager 1 is marked by a vertical dashed line. Below are shown the Sunspot Numbers (SSN) during years 1980–2008. We see that the degree of multifractality falls steadily with distance and is apparently modulated by the solar activity, as noted by Burlaga et al. (2003). Macek & Wawrzaszek (2009) have already demonstrated that the multifractal scaling is asymmetric in the outer heliosphere. Now, the degree of asymmetry A of this multifractal spectrum in the heliosphere as a function of the phases of solar cycles is shown in Figure 17 taken from (Macek et al., 2011); the value $A = 1$ (dotted) corresponds to the one-scale symmetric model. One sees that in the heliosphere only one of three points above unity is at large distances from the Sun. In fact, inside the outer heliosphere prevalently $A < 1$ and only once (during the declining phase) the left-skewed spectrum ($A > 1$) was clearly observed. Anyway, it seems that the right-skewed spectrum ($A < 1$) before the crossing of the termination shock is preferred. As expected the multifractal scaling is asymmetric before shock crossing with the calculated degree of asymmetry at distances $70 - 90$ AU equal to $A = 0.47 - 0.96$. It also seems that the asymmetry is probably changing when crossing the termination shock ($A = 1.0 - 1.5$)

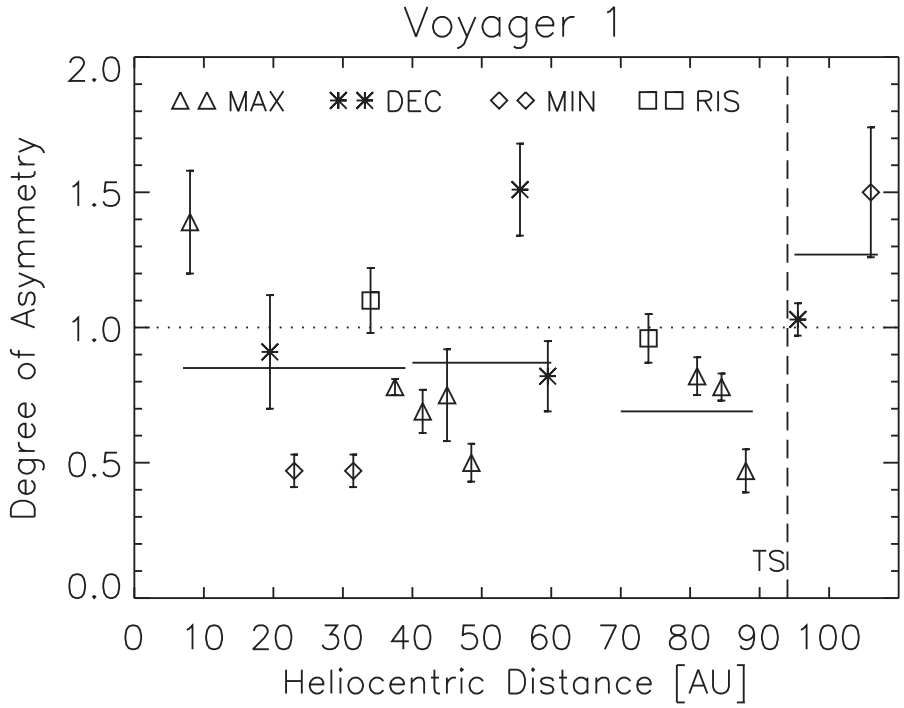

Fig. 17. The degree of asymmetry A of the multifractal spectrum in the heliosphere as a function of the heliospheric distance during solar minimum (MIN) and solar maximum (MAX), declining (DEC) and rising (RIS) phases of solar cycles with the corresponding averages denoted by continuous lines; the value $A = 1$ (dotted) corresponds to the one-scale symmetric model. The crossing of the termination shock (TS) by Voyager 1 is marked by a vertical dashed line.

as is also illustrated in Figure 15, but owing to large errors bars and a very limited sample, symmetric spectrum is still locally possible in the heliosheath (cf. Burlaga & Ness, 2010).

4.3 Degree of Multifractality and Asymmetry

For comparison, the values calculated from the papers by Burlaga et al. (2006) and Burlaga & Ness (2010) (LB) and Macek et al. (2011) are also given in Figure 18 One sees that the degree of multifractality for fluctuations of the interplanetary magnetic field strength obtained from independent types of studies are in surprisingly good agreement; generally these values are smaller than that for the energy rate transfer in the turbulence cascade ($\Delta = 2 - 3$), Table 2 taken from (Macek & Wawrzaszek, 2009). Moreover, it is worth noting that our values obtained before the shock crossing, $\Delta = 0.4 - 0.7$, are somewhat greater than those for the heliosheath Δ = 0.3–0.4. This confirms the results presented by Burlaga et al. (2006) and Burlaga & Ness (2010). In this way we have provided a supporting evidence that the magnetic field behavior in the outer heliosphere, even in a very deep heliosphere, may exhibit a multifractal scaling, while in the heliosheath smaller values indicate possibility toward a monofractal behavior, implying roughly the same density of the probability measure.

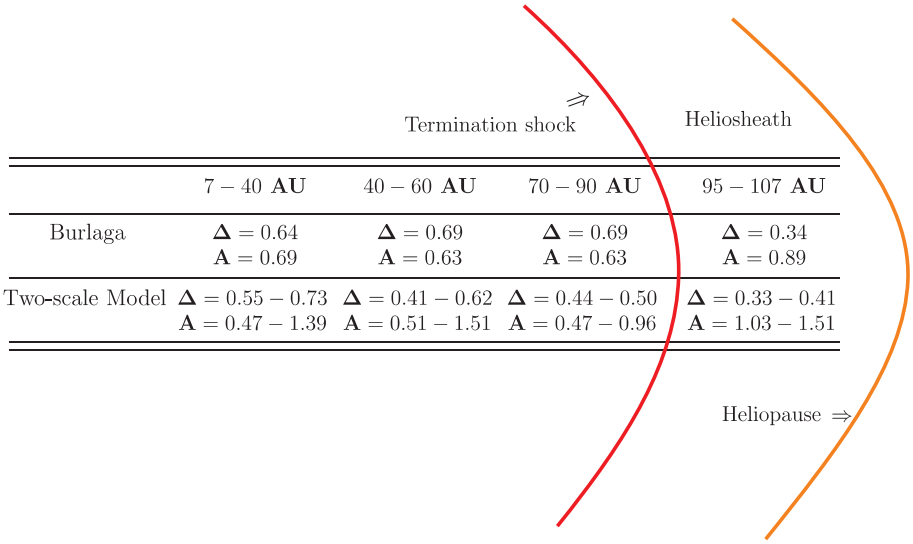

	$7-40$ **AU**	$40-60$ **AU**	$70-90$ **AU**	$95-107$ **AU**
Burlaga	$\mathbf{\Delta}=0.64$ $\mathbf{A}=0.69$	$\mathbf{\Delta}=0.69$ $\mathbf{A}=0.63$	$\mathbf{\Delta}=0.69$ $\mathbf{A}=0.63$	$\mathbf{\Delta}=0.34$ $\mathbf{A}=0.89$
Two-scale Model	$\mathbf{\Delta}=0.55-0.73$ $\mathbf{A}=0.47-1.39$	$\mathbf{\Delta}=0.41-0.62$ $\mathbf{A}=0.51-1.51$	$\mathbf{\Delta}=0.44-0.50$ $\mathbf{A}=0.47-0.96$	$\mathbf{\Delta}=0.33-0.41$ $\mathbf{A}=1.03-1.51$

Fig. 18. Degree of multifractality Δ and asymmetry A for the magnetic field strengths in the outer heliosphere and beyond the termination shock.

5. Conclusions

We have studied the inhomogeneous rate of the transfer of the energy flux indicating multifractal and intermittent behavior of solar wind turbulence in the inner and outer heliosphere also out of ecliptic and even in the heliosheath. Basically, the generalized dimensions for solar wind are consistent with the generalized p-model for both positive and negative q, but rather with different scaling parameters for sizes of eddies, while the usual p-model can only reproduce the spectrum for $q \geq 0$. In fact, using our weighted two-scale Cantor set model, which is a convenient tool to investigate the asymmetry of the multifractal spectrum, we confirm the characteristic shape of the universal multifractal singularity spectrum; as seen in Figures 15, $f(\alpha)$ is an downward concave function of scaling indices α.

By investigating Ulysses data we have shown that the degree of multifractality and asymmetry of the fast solar wind exhibit latitudinal dependence with some symmetry with respect to the ecliptic plane. Both quantities seem to be correlated during solar minimum for latitudes below 70°. The multifractal singularity spectra become roughly symmetric. The minimum intermittency is observed at mid-latitudes and is possibly related to the transition from the region where the interaction of the fast and slow streams takes place to a more homogeneous region of the pure fast solar wind.

Basically, here for the first time we show that the degree of multifractality for magnetic field fluctuations of the solar wind falls steadily with the distance from the Sun and seems to be modulated by the solar activity. Moreover, in contrast to the right-skewed asymmetric spectrum with singularity strength $\alpha > 1$ inside the heliosphere, the spectrum becomes more left-skewed, $\alpha < 1$, or approximately symmetric after the shock crossing in the heliosheath, where the plasma is expected to be roughly in equilibrium in the transition to the interstellar medium. In particular, we also confirm the results obtained by Burlaga et al. (2006) that

before the shock crossing, especially during solar maximum, turbulence is more multifractal than that in the heliosheath.
Hence we hope that our new more general asymmetric multifractal model could shed light on the nature of turbulence and we therefore propose this model as a useful tool for analysis of intermittent turbulence in various environments.

Acknowledgments

This work has been supported by the Polish National Science Centre (NCN) and the Ministry of Science and Higher Education (MNiSW) through Grant NN 307 0564 40. We would like to thank the plasma plasma instruments teams of Helios, Advanced Composition Explorer, Ulysses, and Voyager, and also the magnetic field instruments teams of ACE and Voyager missions for providing experimental data.

6. References

Alexandrova, O., Carbone, V., Veltri, P. & Sorriso-Valvo, L. (2007). Solar wind Cluster observations: Turbulent spectrum and role of Hall effect, *Planet. Space Sci.* **55**: 2224–2227.

Bruno, R., Carbone, V., Sorriso-Valvo, L. & Bavassano, B. (2003). Radial evolution of solar wind intermittency in the inner heliosphere, *J. Geophys. Res.* **108**.

Bruno, R., Carbone, V., Veltri, P., Pietropaolo, E. & Bavassano, B. (2001). Identifying intermittency events in the solar wind, *Planet. Space Sci.* **49**: 1201–1210.

Burlaga, L. F. (1991b). Multifractal structure of the interplanetary magnetic field - Voyager 2 observations near 25 AU, 1987-1988, *Geophys. Res. Lett.* **18**: 69–72.

Burlaga, L. F. (1995). *Interplanetary magnetohydrodynamics*, New York: Oxford Univ. Press.

Burlaga, L. F. (2001). Lognormal and multifractal distributions of the heliospheric magnetic field, *J. Geophys. Res.* **106**: 15917–15927.

Burlaga, L. F. (2004). Multifractal structure of the large-scale heliospheric magnetic field strength fluctuations near 85 AU, *Nonlin. Processes Geophys.* **11**: 441–445.

Burlaga, L. F. & Klein, L. W. (1986). Fractal structure of the interplanetary magnetic field, *J. Geophys. Res.* **91**: 347–350.

Burlaga, L. F. & Ness, N. F. (2010). Sectors and large-scale magnetic field strength fluctuations in the heliosheath near 110 AU: Voyager 1, 2009, *Astrophys. J.* **725**: 1306–1316.

Burlaga, L. F., Ness, N. F. & Acuña, M. H. (2006). Multiscale structure of magnetic fields in the heliosheath, *J. Geophys. Res.* **111**: A09112.

Burlaga, L. F., Ness, N. F., Acuña, M. H., Lepping, R. P., Connerney, J. E. P., Stone, E. C. & McDonald, F. B. (2005). Crossing the termination shock into the heliosheath: Magnetic fields, *Science* **309**: 2027–2029.

Burlaga, L. F., Perko, J. & Pirraglia, J. (1993). Cosmic-ray modulation, merged interaction regions, and multifractals, *Astrophys. J.* **407**: 347–358.

Burlaga, L. F., Wang, C. & Ness, N. F. (2003). A model and observations of the multifractal spectrum of the heliospheric magnetic field strength fluctuations near 40 AU, *Geophys. Res. Lett.* **30**: 50–1.

Carbone, V. (1993). Cascade model for intermittency in fully developed magnetohydrodynamic turbulence, *Phys. Rev. Lett.* **71**: 1546–1548.

Chhabra, A. B., Meneveau, C., Jensen, R. V. & Sreenivasan, K. R. (1989). Direct determination of the f(α) singularity spectrum and its application to fully developed turbulence, *Phys. Rev. A* **40**(9): 5284–5294.

Chhabra, A. & Jensen, R. V. (1989). Direct determination of the f(α) singularity spectrum, *Phys. Rev. Lett.* **62**(12): 1327–1330.

Frisch, U. (1995). *Turbulence. The legacy of A.N. Kolmogorov*, Cambridge: Cambridge Univ. Press.

Frisch, U., Sulem, P.-L. & Nelkin, M. (1978). A simple dynamical model of intermittent fully developed turbulence, *J. Fluid Mech.* **87**: 719–736.

Goldstein, B. E., Smith, E. J., Balogh, A., Horbury, T. S., Goldstein, M. L. & Roberts, D. A. (1995). Properties of magnetohydrodynamic turbulence in the solar wind as observed by Ulysses at high heliographic latitudes, *Geophys. Res. Lett.* **22**: 3393–3396.

Grassberger, P. (1983). Generalized dimensions of strange attractors, *Phys. Lett. A* **97**: 227–230.

Grassberger, P. & Procaccia, I. (1983). Measuring the strangeness of strange attractors, *Physica D* **9**: 189–208.

Halsey, T. C., Jensen, M. H., Kadanoff, L. P., Procaccia, I. & Shraiman, B. I. (1986). Fractal measures and their singularities: The characterization of strange sets, *Phys. Rev. A* **33**(2): 1141–1151.

Hentschel, H. G. E. & Procaccia, I. (1983). The infinite number of generalized dimensions of fractals and strange attractors, *Physica D* **8**: 435–444.

Horbury, T. S., Balogh, A., Forsyth, R. J. & Smith, E. J. (1996). Magnetic field signatures of unevolved turbulence in solar polar flows, *J. Geophys. Res.* **101**: 405–413.

Jensen, M. H., Kadanoff, L. P. & Procaccia, I. (1987). Scaling structure and thermodynamics of strange sets, *Phys. Rev. A* **36**: 1409–1420.

Kolmogorov, A. (1941). The local structure of turbulence in incompressible viscous fluid for very large Reynolds' numbers, *Akademiia Nauk SSSR Doklady* **30**: 301–305.

Kraichnan, R. H. (1965). Inertial-range spectrum of hydromagnetic turbulence, *Phys. Fluids* **8**: 1385–1387.

Lamy, H., Wawrzaszek, A., Macek, W. M. & Chang, T. (2010). New multifractal analyses of the solar wind turbulence: Rank-ordered multifractal analysis and generalized two-scale weighted Cantor set model, *Twelfth International Solar Wind Conference* **1216**: 124–127.

Macek, W. M. (1998). Testing for an attractor in the solar wind flow, *Physica D* **122**: 254–264.

Macek, W. M. (2002). Multifractality and chaos in the solar wind, *in* S. Boccaletti, B. J. Gluckman, J. Kurths, L. M. Pecora & M. L. Spano (eds), *Experimental Chaos*, Vol. 622 of *American Institute of Physics Conference Series*, pp. 74–79.

Macek, W. M. (2003). The multifractal spectrum for the solar wind flow, *in* M. Velli, R. Bruno, F. Malara & B. Bucci (eds), *Solar Wind Ten*, Vol. 679 of *American Institute of Physics Conference Series*, pp. 530–533.

Macek, W. M. (2006a). Modeling multifractality of the solar wind, *Space Sci. Rev.* **122**: 329–337.

Macek, W. M. (2006b). Multifractal solar wind, *Academia* **3**: 16–18.

Macek, W. M. (2007). Multifractality and intermittency in the solar wind, *Nonlin. Processes Geophys.* **14**: 695–700.

Macek, W. M., Bruno, R. & Consolini, G. (2005). Generalized dimensions for fluctuations in the solar wind, *Phys. Rev. E* **72**(1).

Macek, W. M., Bruno, R. & Consolini, G. (2006). Testing for multifractality of the slow solar wind, *Adv. Space Res.* **37**: 461–466.

Macek, W. M. & Redaelli, S. (2000). Estimation of the entropy of the solar wind flow, *Phys. Rev. E* **62**: 6496–6504.

Macek, W. M. & Szczepaniak, A. (2008). Generalized two-scale weighted Cantor set model for solar wind turbulence, *Geophys. Res. Lett.* **35**.

Macek, W. M. & Wawrzaszek, A. (2009). Evolution of asymmetric multifractal scaling of solar wind turbulence in the outer heliosphere, *J. Geophys. Res.* **114**(13).

Macek, W. M. & Wawrzaszek, A. (2011a). Multifractal structure of small and large scales fluctuations of interplanetary magnetic fields, *Planet. Space Sci.* **59**: 569–574.

Macek, W. M. & Wawrzaszek, A. (2011b). Multifractal two-scale cantor set model for slow solar wind turbulence in the outer heliosphere during solar maximum, *Nonlin. Processes Geophys.* **18**(3): 287–294.
URL: *http://www.nonlin-processes-geophys.net/18/287/2011/*

Macek, W. M., Wawrzaszek, A. & Carbone, V. (2011). Observation of the multifractal spectrum at the termination shock by Voyager 1, *Geophys. Res. Lett.* **38**.

Macek, W. M., Wawrzaszek, A. & Hada, T. (2009). Multiscale multifractal intermittent turbulence in space plasmas, *J. Plasma Fusion Res. SERIES* **8**: 142–147.

Mandelbrot, B. B. (1989). Multifractal measures, especially for the geophysicist, *Pure Appl. Geophys.* **131**: 5–42.

Marino, R., Sorriso-Valvo, L., Carbone, V., Noullez, A., Bruno, R. & Bavassano, B. (2008). Heating the solar wind by a magnetohydrodynamic turbulent energy cascade, *Astrophys. J.* **677**: L71–L74.

Marsch, E., Tu, C.-Y. & Rosenbauer, H. (1996). Multifractal scaling of the kinetic energy flux in solar wind turbulence, *Ann. Geophys.* **14**: 259–269.

Meneveau, C. & Sreenivasan, K. R. (1987). Simple multifractal cascade model for fully developed turbulence, *Phys. Rev. Lett.* **59**: 1424–1427.

Meneveau, C. & Sreenivasan, K. R. (1991). The multifractal nature of turbulent energy dissipation, *J. Fluid Mech.* **224**: 429–484.

Ott, E. (1993). *Chaos in dynamical systems*, Cambridge: Cambridge Univ. Press.

Schwenn, R. (1990). *Large-Scale Structure of the Interplanetary Medium*, Vol. 20, Berlin: Springer-Verlag, pp. 99–182.

Smith, E. J., Balogh, A., Lepping, R. P., Neugebauer, M., Phillips, J. & Tsurutani, B. T. (1995). Ulysses observations of latitude gradients in the heliospheric magnetic field, *Adv. Space Res.* **16**: 165.

Sorriso-Valvo, L., Carbone, V., Veltri, P., Consolini, G. & Bruno, R. (1999). Intermittency in the solar wind turbulence through probability distribution functions of fluctuations, *Geophys. Res. Lett.* **26**: 1801–1804.

Sorriso-Valvo, L., Marino, R., Carbone, V., Noullez, A., Lepreti, F., Veltri, P., Bruno, R., Bavassano, B. & Pietropaolo, E. (2007). Observation of inertial energy cascade in interplanetary space plasma, *Phys. Rev. Lett.* **99**(11): 115001.

Szczepaniak, A. & Macek, W. M. (2008). Asymmetric multifractal model for solar wind intermittent turbulence, *Nonlin. Processes Geophys.* **15**: 615–620.

Wawrzaszek, A. & Macek, W. M. (2010). Observation of the multifractal spectrum in solar wind turbulence by Ulysses at high latitudes, *J. Geophys. Res.* **115**(14).

Yordanova, E., Balogh, A., Noullez, A. & von Steiger, R. (2009). Turbulence and intermittency in the heliospheric magnetic field in fast and slow solar wind, *J. Geophys. Res.* **114**(A13).